High latitude molecular clouds - Distances and extinctions

Magnani, L.; Vries, C.P. de

Astron. Astrophys. 168, 271–283 (1986)

ASTRONOMY AND ASTROPHYSICS

High latitude molecular clouds: distances and extinctions

L. Magnani[1] **and C.P. de Vries**[2]

[1] Astronomy Program, University of Maryland, College Park, MD 20742 USA
[2] Sterrewacht Leiden, P.O. Box 9513, 2300 RA Leiden, The Netherlands

Received April 14, accepted July 16, 1986

Summary. Automated star counts are used to determine the distances to a number of the high latitude ($|b|>25°$) molecular clouds. Distances to three of the clouds are obtained and range from ~ 100 pc to ~ 175 pc; upper limits are obtained for the distances to five other objects and range from $\leqq 125$ pc to $\leqq 275$ pc. These results are consistent with the previously determined average distance (~ 100 pc) based on the velocity dispersion and scale height of the ensemble of clouds: the high latitude molecular clouds are features of the local interstellar medium.

Because all of the high latitude clouds correspond to IRAS infrared cirrus features, the distance estimates in this paper locate at least some of the IRAS cirrus features in the solar neighbourhood. In addition, cloud 20, which contains a pair of T-Tauri stars, is at a distance of <125 pc and may be as close as 75 pc. This object appears to be the nearest star forming region to the Sun.

The extinction averaged over the area bounded by the lowest CO contour is very low, with A_v ranging from $0^m.3$ to $0^m.9$. Even the 0.4 to 1 square degrees areas chosen as the most obscured regions for distance determinations show extinctions from $0^m.45$ to $2^m.1$ A_v magnitudes, substantially less than the most obscured regions of typical dark molecular clouds.

Key words: distances – the Galaxy: solar neighbourhood – interstellar medium: clouds: extinction

1. Introduction

The presence of significant quantities of CO at high Galactic latitudes ($|b|\geqq 25°$) was first reported by Blitz et al. (1984; hereafter Paper I). Concurrently, 100 μm data from the Infrared Astronomical Satellite (IRAS) satellite revealed the presence of a considerable number of cold, diffuse, dust clouds at high galactic latitude: the infrared cirrus (Low et al., 1984). A comparison of the two surveys establishes that all the high latitude molecular clouds can be identified with the cores of IRAS infrared cirrus although not all areas of extended 100 μm emission show detectable molecular emission (Weiland et al., 1986).

Paper I argues that the low velocity dispersion of the ensemble of high latitude molecular clouds ($\sim 5.7\,\mathrm{km\,s^{-1}}$) indicates that they, as a group, are at an average distance of ~ 100 pc. To confirm this result, direct distance determinations to eight of the molecular complexes were made from a program of automated star counts. Because the high latitude molecular clouds are clearly associated with the infrared cirrus, the distance determinations in this paper locate at least some of the high latitude cirrus in the local interstellar medium.

Section 2 of the paper briefly describes the method of star counts to determine distances and extinctions, the data reduction procedures and calibration employed, and some of the problems encountered. The distances and extinctions for individual objects are discussed in Sect. 3. Section 4 presents the conclusions of this study.

2. Method

2.1. Theory

The use of star counts to determine distances to dust clouds is an established astronomical technique, described in the classic work by Bok (1937), *The Distribution of Stars in Space*. Basically, the method involves comparing the number of stars of a particular magnitude in a field obscured by an absorbing cloud to the number of stars of the same magnitude in a comparison, obscuration-free field. The presence of obscuring material will produce a decrease in the number of stars per magnitude interval in the obscured field. This quantity can be related to the distance and extinction of the obscuring cloud if the luminosity function is known.

Following the treatment in Bok (1937), the number of stars of apparent magnitude m in a direction (l, b), denoted by $A(l, b, m)$, is related to the stellar luminosity function, Φ_r by

$$A(l,b,m)=\omega \int_0^{\infty} r^2 \Phi_r(m+5-5\log r-a(r))\,dr\,, \qquad (1)$$

where ω is the solid angle surveyed in obtaining $A(l, b, m)$, and $a(r)$ is the absorption in magnitudes as a function of the distance r.

Because it cannot be assumed that the luminosity function remains the same throughout space, the integral equation must be solved for the distance and extinction numerically. Many techniques have been used to obtain a solution. A particularly straightforward method involves Wolf diagrams (Wolf, 1923), plots of the apparent stellar magnitude, m, versus log $N(m)$ where $N(m)\equiv \int_{-\infty}^{m} A(m)\,dm$. Bok (1937) explains how Wolf diagrams are employed to determine the distance and extinction to an obscuring cloud. Wolf diagrams generated by using a realistic luminosity

Send offprint requests to: L. Magnani

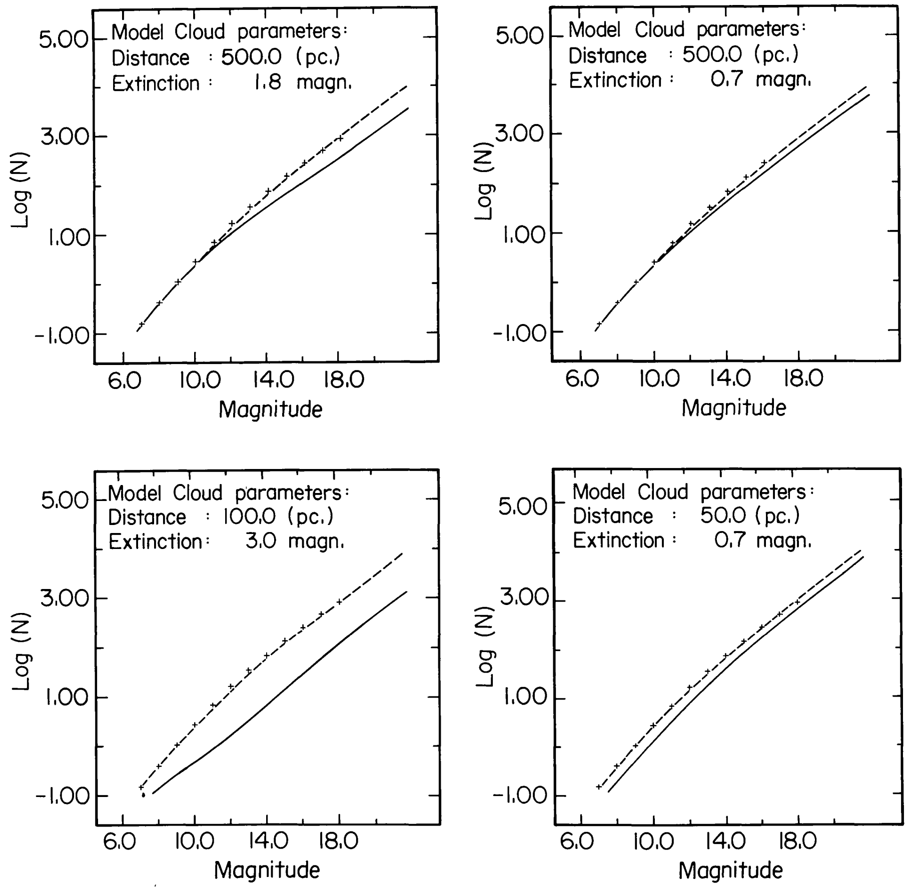

Fig. 1. Actual Wolf diagram with the stellar density function described in the text. The dashed line shows the calibrated stellar density function for a given line of sight and the crosses show the van Rhijn (1929) data for the line of sight. Log (N) is the total number of stars brighter than a magnitude m. The solid line shows the effects of a model obscuring cloud with the given distances and extinctions. Unless the cloud has sizeable extinction and is also distant (upper left-hand corner), the turnoff occurs at magnitudes brighter than 10 where the star count data are virtually non-existent

function and a model obscuring cloud at varying distances with differing extinctions are shown in Fig. 1. With a knowledge of the general luminosity function (e.g. Bahcall and Soneira, 1980) and the relative stellar density function, theoretical Wolf diagrams for various values of the distance and extinction due to an obscuring cloud are produced. These diagrams are then compared to the actual star counts to determine which distance and extinction yield the best fit to the data.

2.2. *Data reduction*

The star count data were obtained at the University of Leiden using the Leiden Observatory Astroscan (described in more detail by Swaans, 1981). The digitizing of nearly 1/3 of a Palomar Sky Survey (POSS) plate is accomplished in approximately 65 h. The data were recorded at a resolution of 20 μm corresponding to an angular resolution on the plates of 1.″34.

The calibration for transforming the data elements into photographic densities is accomplished with a set of 13 neutral density filters ranging from 0.04D to 3.72D. These filters are scanned before digitizing a new plate to account for lamp and other equipment changes over time. The density repeatability of the system is better than 0.01 D.

Blue POSS plates are chosen for the star counts because the extinction is greater than on red plates. The software is designed to divide the $244 \times 231\ \mathrm{mm}^2$ available plate surface into an 11×11 element array and then to scan each individual element (termed a "matrix") before moving to the next matrix. In this fashion, the entire plate is digitized and the information stored on magnetic tape.

Because of the good correlation between the high latitude molecular clouds and optical emission visible on the blue or red POSS plates (Magnani et al., 1985; hereafter Paper II), it is necessary to identify and remove the luminous background of the field to avoid confusion and to produce a complete, homogeneous data file of stellar objects. An automated star counting program especially designed to operate reliably in nebulous regions has been developed by de Vries (1984, 1986).

A background density is computed using the lowest photographic density pixels in a sub-grid of area $S \times S$ where S is some length scale greater than the diameter of most stellar images. The quantity S was usually taken to be 1.5 mm (corresponding to 1.′68). Changing the size of S does not significantly alter the star count data.

The $S \times S$ areas cover the entire scanned portion of the plate. The respective background samples are convolved with a gaussian over a $3S \times 3S$ area in the two spatial dimensions of the plate to create a smooth variation of background density across the entire plate. After the background is calculated in this fashion, it is subtracted from the entire digitized image of the plate.

Once the background is removed, the object detection program scans the data pixels at four decreasing threshold levels of photographic density in order to separate merged objects. At each level, all adjacent pixels above the threshold are stored as an object and placed in a file. The files are then cross-correlated to produce a file containing the object and information pertinent to the object; i.e. the major and minor axes of the object's lowest contour and the relative position of the maximum density within the object. In this manner, different types of objects such as stellar images, small filaments, elongated galaxies, and dusthairs can be identified.

The brightness of individual stars in a scanned field is stored on magnetic tape in terms of a photometric parameter which is chosen so as to minimize the uncertainty in the relation between the photometric density of a star and the photographic magnitude of the star. The details of how the photometric parameter is defined and constructed from the digitized data are presented in de Vries (1986). For the purposes of this paper, it is only necessary to state that this parameter can be directly related to stellar magnitudes by the calibration technique described in Sect. 2.3.

The stellar density data were later convolved with a Gaussian beam to yield an effective resolution of 8′. This convolution smoothes the star cound data to reduce the noise and allows the direct (future) comparison between the stellar density data and the IRAS Spline1 products which also show a resolution of 8′.

2.3. Calibration

In order to create Wolf diagrams for the digitized regions, the photometric density of individual stars must be converted to a photographic magnitude. Because the POSS plates are uncalibrated, this calibration is accomplished by comparing the stellar density data in an obscuration-free field to the star counts given in the van Rhijn (1929) tables for the line of sight in question. Although the van Rhijn (1929) tables were obtained from photographic plates, the spectral sensitivity of these plates is similar to the blue POSS plates used for the star counts in this work. Errors due to the differing spectral sensitivities are therefore expected to be negligible. Theoretical Wolf diagrams are then created using models of the stellar density distribution and the interstellar extinction. The parameters of the models are varied until the stellar distribution [m versus $\log N(m)$] matches the distribution given in the van Rhijn (1929) tables for the given line of sight.

To obtain a realistic function $A(m)$, models for $\Phi_r(M)$ and $a(r)$ are defined. To model $\Phi_r(M)$, the galactic structure is taken into account. Because the clouds used in this study are at high galactic latitudes, a simple model is used: For $\Phi_r(M)$ in the galactic plane, the function $\Phi_0(M)$ is taken from Allen (1973). Outside the galactic plane, $\Phi_0(M)$ is is modified by assigning a variable scale height, $h(M)$, to stars of different luminosities, so that

$$\Phi_r(M) = \Phi_0(M) \exp\left[\frac{-r\sin(b)}{h(M)}\right]. \tag{2}$$

The scale height function $h(M)$ we employ is shown in Table 1. A first effect of this modification in Φ_r is to decrease the slope of $\log A(m)$. In addition, the curve will flatten towards faint magnitudes because the line of sight at high galactic latitudes ultimately leaves the galactic layer. These effects will be greater for higher galactic latitudes.

To model the extinction along the line of sight, $a(r)$ is divided into a general interstellar space extinction term, $a_s(r)$, and an extinction term due to concentrations of obscuring material, $a_c(r)$. For calibrating the star count data, an obscuration-free field with $a_c(r) = 0$ is chosen and the space extinction is assumed to be a constant A_s magnitudes per kpc so that $a_s(r) = A_s r$. For an infinite and constant density of stars, the effect of A_s is to decrease the slope in the m versus $\log A(m)$ relation.

The luminosity function employed in the stellar density distribution model is from Allen (1973). Although the luminosity function of Bahcall and Soneira (1980) is perhaps more reliable since it is based on a compendium of all previous determinations of luminosity functions including some data not available in 1973, the differences between the two luminosity functions are small. Using the Bahcall and Soneira (1980) luminosity function would not change appreciably the results of this paper.

Table 1. Number of stars $\log N$ in the solar neighbourhood and scaleheights (h_0) as functions of absolute magnitude (M_v) used in the stellar density models. These data are taken from Allen (1973)

M_v	$\log(N)+10$	h_0 (pc)	Notes
−4	3.63	50	
−2	4.77	80	
0	5.87	120	
2	6.70	160	
4	7.19	270	
6	7.47	450	
8	7.61	800	
10	7.81	2000	
12	7.97	4000	
14	8.06	8000	a
16	8.08	8000	a
18	7.95	8000	a
20	7.60	8000	a
22	6.90	8000	a

[a] "Extrapolated" for use in this work

2.4. Wolf diagrams

Once the stellar density distribution is correctly parametrized and the photometric parameter is calibrated, the most obscured 0.4 to 1.0 square degrees area within the molecular emission region is chosen. The value of the extinction obtained from the Wolf diagrams and listed in Table 3 is therefore an upper limit to the extinction (in blue magnitudes) averaged over the rest of the molecular cloud. The calibrated photometric parameter is then used to convert the number of stars of a given photometric density in the obscured field to the number of stars per blue magnitude.

The resulting m vs. $\log N(m)$ plot for the obscured region is compared with theoretical Wolf diagrams for the particular stellar distribution model employed with obscuring clouds of various extinction and at various distances. A goodness of fit parameter defined as $[(\log N(m)_{\rm data}) - (\log N(m)_{\rm model})]^2$ and weighted by N is employed to choose which value of the extinction fits the data best for a cloud at 100 pc. Because of frequent problems with the star count data at magnitudes greater than 17 (see Sect. 2.6) only the data for magnitudes $\leqq 17$ are used in determining the best fit extinction. Once the extinction in the obscured field is determined, the goodness of fit parameter is used to determine which value of the distance in 50 pc intervals best fits the data.

We found that additional iterations did not produce significantly different extinctions or distances to the cloud regions although the values of the goodness of fit parameter changed slightly. The value for the extinction of the obscured region determined after successive iterations changes by less than $0^{\rm m}\!.2$. Varying the extinction of the obscured region within this range does not change the value of the distance determined by the goodness of fit parameter method.

Table 2

Cloud (Paper II)	α (1950)	δ	l	b	Distance (pc)	A_v extinction: Obscured region* $m \leqq 17$	$m \leqq 20$	Entire cloud
7[a]	2 19.6	19 40.0	150.4	−38.1	125 ± 50	0ᵐ9	0ᵐ7	0ᵐ5
16	3 17.7	10 30.0	171.7	−37.7	100 ± 50	1.9	1.4	0.9
18	3 59.8	01 10.0	189.1	−36.0	≲175	1.1	0.8	0.8
20	4 33.0	−14 20.0	210.9	−36.5	≲125	1.4	1.0	0.8
26	8 02.8	60 43.0	156.4	32.6	175 ± 50	0.6	0.6	0.7
32[b]	9 21.8	67 05.0	146.4	39.6	≲275	0.5	0.5	0.3
55[c]	23 05.9	14 49.0	89.2	−40.9	≲175	0.5	0.5	0.4
55A	23 50.7	20 40.0	105.1	−39.9	≲275	0.5	0.5	–

* The area chosen as the obscured field in the Wolf diagrams
[a] Cloud 8 is located within 0°5 of cloud 7
[b] Cloud 31 is located within 0°5 of cloud 32
[c] Cloud 54 is located within 0°5 of cloud 55

Table 3. Goodness of fit parameter

Cloud	Dist. (pc)	A_B (ᵐ)	Cutoff 15ᵐ	Cutoff 17ᵐ	Cloud	Dist. (pc)	A_B (ᵐ)	Cutoff 15ᵐ	Cutoff 17ᵐ
7	0	1.15	$0.65\ 10^{-2}$	0.11	26	0	0.80	$0.91\ 10^{-2}$	0.16
	50	1.15	$0.64\ 10^{-2}$	0.11		50	0.80	$0.88\ 10^{-2}$	0.15
	100	1.15	$0.58\ 10^{-2}$	0.10		100	0.80	$0.74\ 10^{-2}$	0.13
	150	1.15	$0.54\ 10^{-2}$	0.10		150	0.80	$0.64\ 10^{-2}$	0.12
	200	1.15	$0.64\ 10^{-2}$	0.12		200	0.80	$0.65\ 10^{-2}$	0.12
	250	1.15	$0.84\ 10^{-2}$	0.15		250	0.80	$0.75\ 10^{-2}$	0.13
	300	1.15	$0.15\ 10^{-1}$	0.24		300	0.80	$0.11\ 10^{-1}$	0.18
16	0	2.80	$0.71\ 10^{-2}$	0.81	31, 32	0	0.65	$0.59\ 10^{-2}$	0.11
	50	2.80	$0.73\ 10^{-2}$	0.80		50	0.65	$0.60\ 10^{-2}$	0.11
	100	2.80	$0.12\ 10^{-1}$	0.78		100	0.65	$0.62\ 10^{-2}$	0.12
	150	2.80	$0.30\ 10^{-1}$	0.82		150	0.65	$0.69\ 10^{-2}$	0.13
	200	2.80	$0.74\ 10^{-1}$	1.00		200	0.65	$0.82\ 10^{-2}$	0.15
	250	2.80	0.11	1.20		250	0.65	$0.94\ 10^{-2}$	0.16
	300	2.80	0.20	1.70		300	0.65	$0.12\ 10^{-1}$	0.21
18	0	1.40	$0.43\ 10^{-2}$	$0.58\ 10^{-1}$	55	0	0.70	$0.98\ 10^{-2}$	0.16
	50	1.40	$0.44\ 10^{-2}$	$0.59\ 10^{-1}$		50	0.70	$0.10\ 10^{-1}$	0.16
	100	1.40	$0.50\ 10^{-2}$	$0.68\ 10^{-1}$		100	0.70	$0.11\ 10^{-1}$	0.17
	150	1.40	$0.72\ 10^{-2}$	$0.97\ 10^{-1}$		150	0.70	$0.12\ 10^{-1}$	0.19
	200	1.40	$0.13\ 10^{-1}$	0.17		200	0.70	$0.15\ 10^{-1}$	0.23
	250	1.40	$0.18\ 10^{-1}$	0.24		250	0.70	$0.17\ 10^{-1}$	0.25
	300	1.40	$0.32\ 10^{-1}$	0.42		300	0.70	$0.22\ 10^{-1}$	0.31
20	0	1.75	$0.90\ 10^{-2}$	0.27	55A	0	0.55	$0.77\ 10^{-2}$	0.12
	50	1.75	$0.94\ 10^{-2}$	0.27		50	0.55	$0.77\ 10^{-2}$	0.12
	100	1.75	$0.13\ 10^{-1}$	0.32		100	0.55	$0.77\ 10^{-2}$	0.12
	150	1.75	$0.21\ 10^{-1}$	0.42		150	0.55	$0.78\ 10^{-2}$	0.12
	200	1.75	$0.38\ 10^{-1}$	0.65		200	0.55	$0.84\ 10^{-2}$	0.13
	250	1.75	$0.53\ 10^{-1}$	0.84		250	0.55	$0.91\ 10^{-2}$	0.14
	300	1.75	$0.86\ 10^{-1}$	1.30		300	0.55	$0.11\ 10^{-1}$	0.17

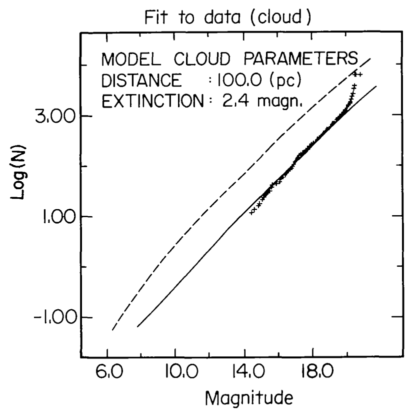

Fig. 2. Wolf diagram of a region in the Taurus dark clouds ($l = 175°$; $b = -19°$). The dashed lines are as described in Fig. 1 and the crosses represent the actual star count data. The distance and extinction of the cloud correspond to accepted values for the region (e.g. Elias, 1978)

The procedure for determining distances and extinctions was checked on two regions whose distances and extinctions have been determined by other investigators; the Taurus dark clouds and the Gum nebula region around RCW 38. The Wolf diagram for the Taurus region is shown in Fig. 2. The best fit to the data is obtained for distances and extinctions of <150 pc and $\sim 2\overset{m}{.}4$, consistent with the values obtained by McCuskey (1941), Adolfsson (1955), and Elias (1978). For the RCW 38 region, the Wolf diagrams indicate a distance of 500 ± 150 pc and an extinction of $\sim 4^m$. The distance agrees with the commonly accepted value for the distance to the Gum nabula (Brandt et al., 1971).

2.5. Extinctions

The extinction maps of the digitized regions are generated using the entire star count data down to the blue POSS plate limit ($\sim$ magnitude 19–20). The extinction maps based on the total star count data give the same extinctions for the areas chosen as the obscured region as the values obtained from the Wolf diagrams using a data cutoff at magnitude 17 for clouds 26, 32, 55, and 55A (see Table 3). Clouds 7, 18, and 20 show a slight difference in the two estimates with the total star count data underestimating the extinction slightly. The region chosen as the obscured area for cloud 16 shows a best fit extinction of $2\overset{m}{.}5$ in the blue using the magnitude 17 data while the total star count data show a blue extinction of $1\overset{m}{.}9$. This difference is substantial only for the higher extinction regions and is most likely a consequence of the upturn at the fainter magnitudes discussed in Sect. 2.6. Only small portions of the clouds have extinctions greater than 1 blue magnitude (see Figs. 3a–g). The star count data extending to the plate limit are therefore used to generate extinction maps for the digitized regions.

Extinctions are obtained from the star count data using the method outlined in Dickman (1978b). The extinction is calculated with respect to the lowest extinction area in the digitized region. At

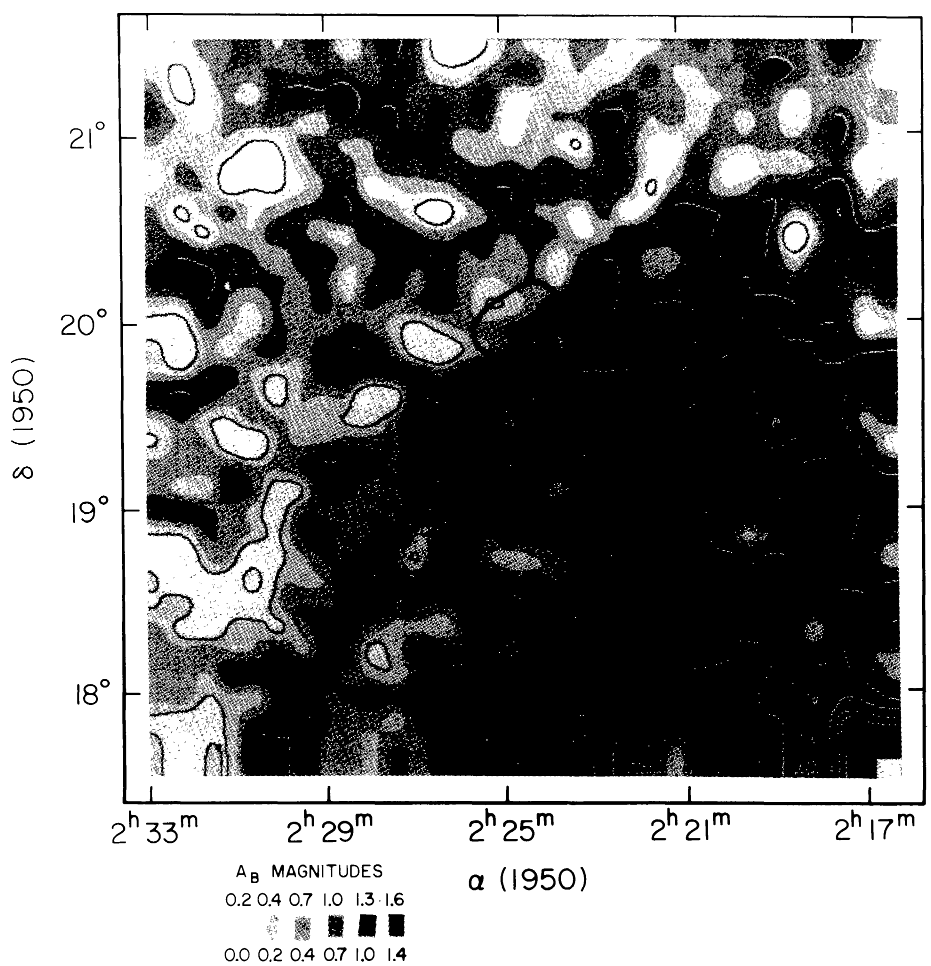

Fig. 3a. The extinction map for the region containing clouds 7 and 8. The gray scale shown at the bottom left is in A_B magnitudes. The heavy black contours show the integrated CO (1 − 0) emission at 0.5, 3.0, 6.0, 9.0, and 12.0 K km s^{-1} intervals for the lines of sight we observed (see Paper II). The extreme right corner of the map ($\alpha < 2^h18^m$ and $\delta \sim 18°$) was not scanned and represents missing data

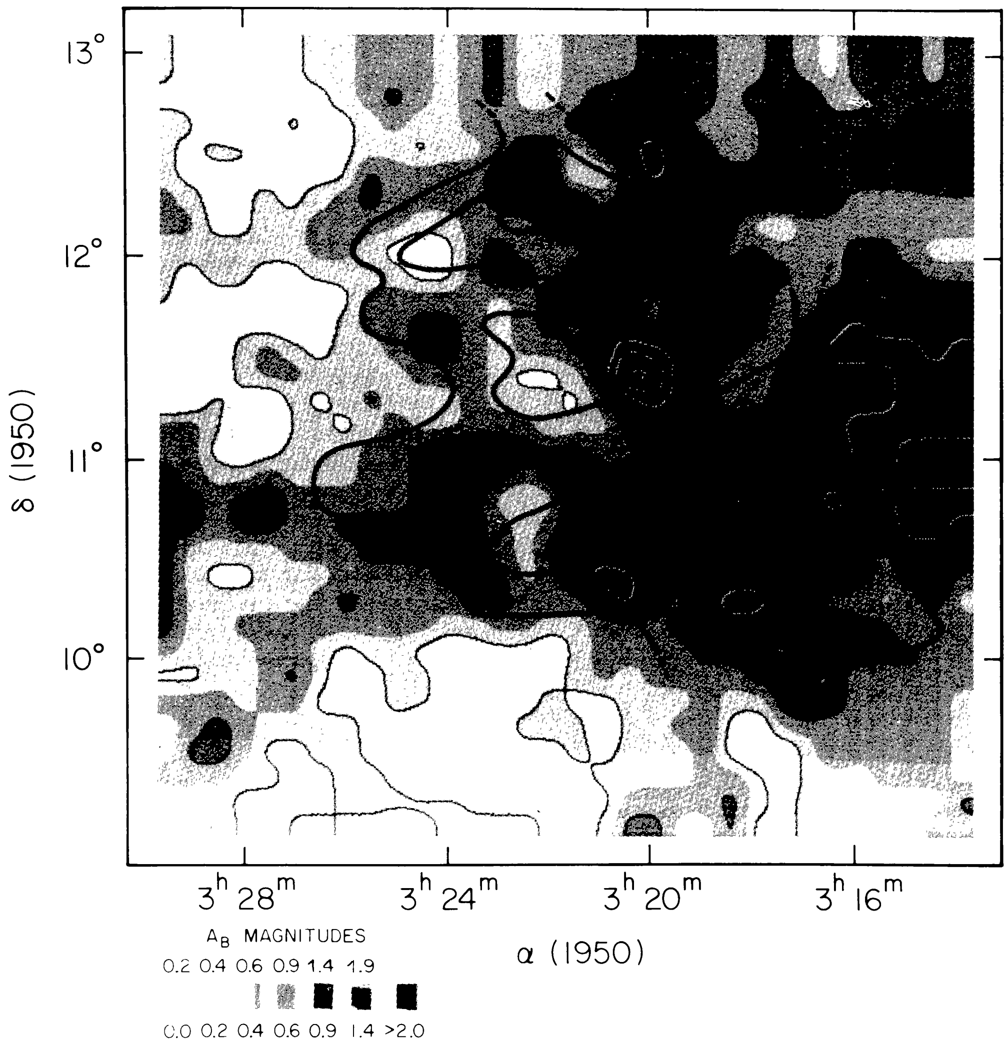

Fig. 3b. Same as Fig. 3a but for the region containing a portion of cloud 16. The heavily obscured area at $\alpha \sim 3^h20^m$ and $\delta \sim 11°20^m$ was not scanned and represents missing data

high galactic latitudes the interstellar extinction accounts for not more than a few tenths of a magnitude in the visual (Lebrun, 1986). The extinctions along any given line of sight are therefore accurate to this background level. If the background is uniform to the resolution of the extinction maps, the extinction obtained from the star counts is then due to the cloud itself. Following Dickman (1978b), the conversion from blue to visual extinctions is accomplished using $A_v = 0.76\,A_B$, and the relative error in the visual extinctions is 0.7 for 8′ resolution.

The CO(1 − 0) integrated antenna temperature maps from Paper II are overlayed on the extinction maps and show correlation between the CO emission and the extinction (see Fig. 3). A quantitative study of this relationship is presented in Magnani et al. (1986).

2.6. Problems

Because the van Rhijn (1929) tables were obtained assuming that there was no interstellar extinction, the presence of extinction in the comparison field can introduce calibration errors in the Wolf diagrams. In particular, the stellar images from the POSS plate are calibrated at a brighter magnitude than they should be. The resulting Wolf diagram will then be shifted to brighter magnitudes leading to an overestimate of the distance and an underestimate of the extinction. However, at the galactic latitudes of the surveyed regions the interstellar extinction is very low ($\leq 0^m.2$; Lebrun, 1986), so this problem should be negligible.

Because of the high galactic latitudes and low extinctions of the high latitude molecular clouds (see Paper II), some galaxies can be expected to be present in the obscured field and certainly in the comparison field. Jarvis and Tyson (1981) present differential star and galaxy counts for $13 < m < 24$ obtained with their automated star counting program which is particularly suited for identifying stars and galaxies. At magnitude 20, the detection limit we set for the blue POSS plates, galaxies account for no more than a few hundred objects in a one square degree field, while stars number a few thousand. In addition, the reduction software we employ will not include any object in the star counts whose major axis is 1.5 times greater than its minor axis. This criterion immediately eliminates all elongated galaxies leaving only small, circular galaxies (about half the total number) to contaminate the star counts; an effect which may be ignored.

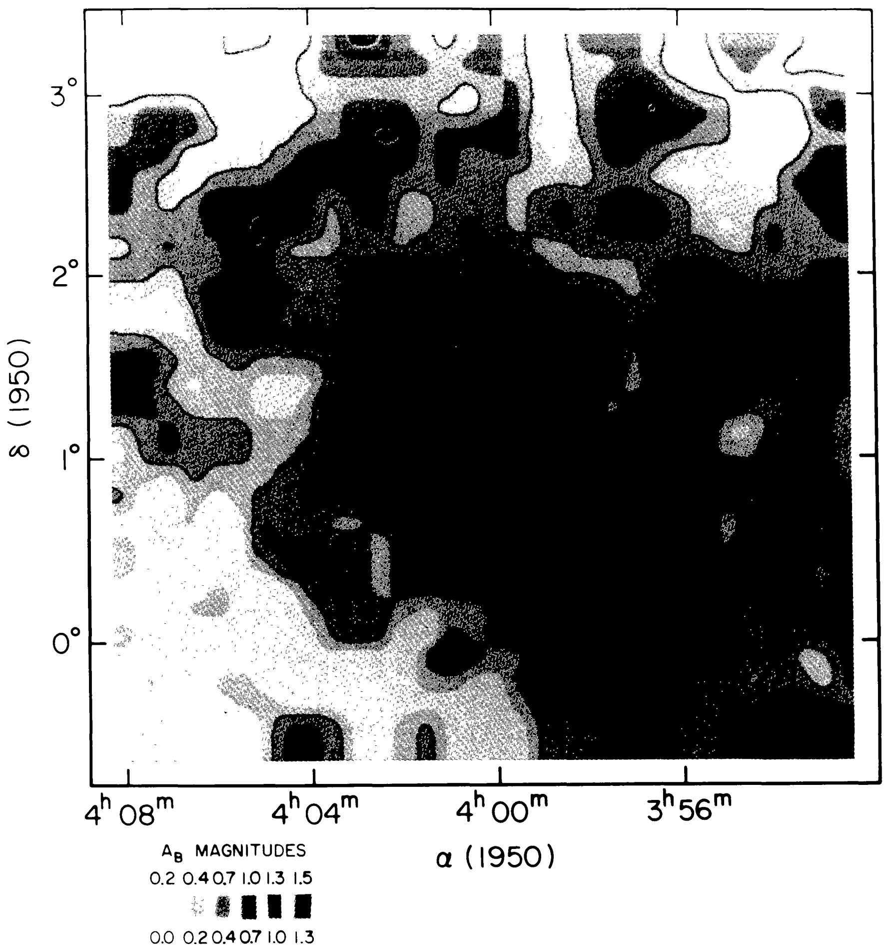

Fig. 3c. Same as Fig. 3a but for the region containing cloud 18 (also known as L 1569)

A problem which sometimes arises in the reduction of the data is an upturn in the faint star data ($m \lesssim 18$) of some of the Wolf diagrams for the obscured regions (e.g. Fig. 5). This upturn or increase in $\log N(m)$ means that there are more faint magnitude objects present in the scanned field than what is predicted by star count analysis. The cause of this increase has not been determined. Some possibilities include the misidentification of plate emulsion inhomogeneities ("noise spikes") as faint stars; the decrease in stellar density at the edges of the POSS plates (where most of the comparison fields are located) due to a gradient in the emulsion and to vignetting in the field; or an error in extrapolating the van Rhijn (1929) tables for magnitudes greater than 18. The tables are complete only to magnitude 18; data for greater magnitudes are obtained by linearly extrapolating the van Rhijn (1929) data. The net result of some or all of the above effects causes the Wolf diagram curve to rise at the fainter magnitudes; this gives the impression that there are more faint stars in the obscured field than is expected.

The various parameters of the theoretical Wolf diagrams may be adjusted to reproduce the rise in the faint star end of the diagrams. This approach is unphysical but it illuminates how the Wolf diagrams are affected by varying some of the parameters of the stellar density distribution model. The possibilities are as follows: 1) Using the same scale height for all types of stars. This approach mimics the effect of the number of stars decreasing as one looks out of the Galactic disk at high latitudes. 2) Cutting off Φ_r at a certain magnitude also simulates the decrease in stars at high latitudes. This effect differs from the first effect because it effectively eliminates all faint nearby stars. 3) A combination of both effects.

Although this problem could not be remedied, distances and extinctions are obtained for the Wolf diagrams by using the data for stars brighter than magnitude 17. It is important to stress that the behavior of the star counts at magnitudes greater than 17 in no way affects the star counts at brighter magnitudes which are calibrated with the data of the van Rhijn (1929) tables. Conclusions based on star count data brighter than or equal to magnitude 17 should be free of these problems *and should therefore yield reliable distance and extinction results.*

The resolution of the above problems cannot resolve the inherent difficulty in applying star count methods to determine the distance to clouds of low extinction: only an upper limit for the distance is frequently obtained if the cloud is less than 150 pc away. Furthermore, the Wolf diagram method is an insensitive distance indicator, so that even for high extinction regions large uncertainties in the distance are inevitable.

For low extinction regions, the lower portion of the curve for the obscured field virtually coincides with the curve for the unobscured field so that a turnoff of the m versus $\log N(m)$ curve from the reference curve is not evident. Since the data for magnitudes less than 12 are subject to large fluctuations (the "noise" level in the counts goes as the square root of the counts; for magnitudes less than 12, typical counts are ~ 10 stars per square degree), it is impossible in most cases to determine the actual distance; only an upper limit to the distance is obtained. In these instances, an accurate distance can only be obtained by

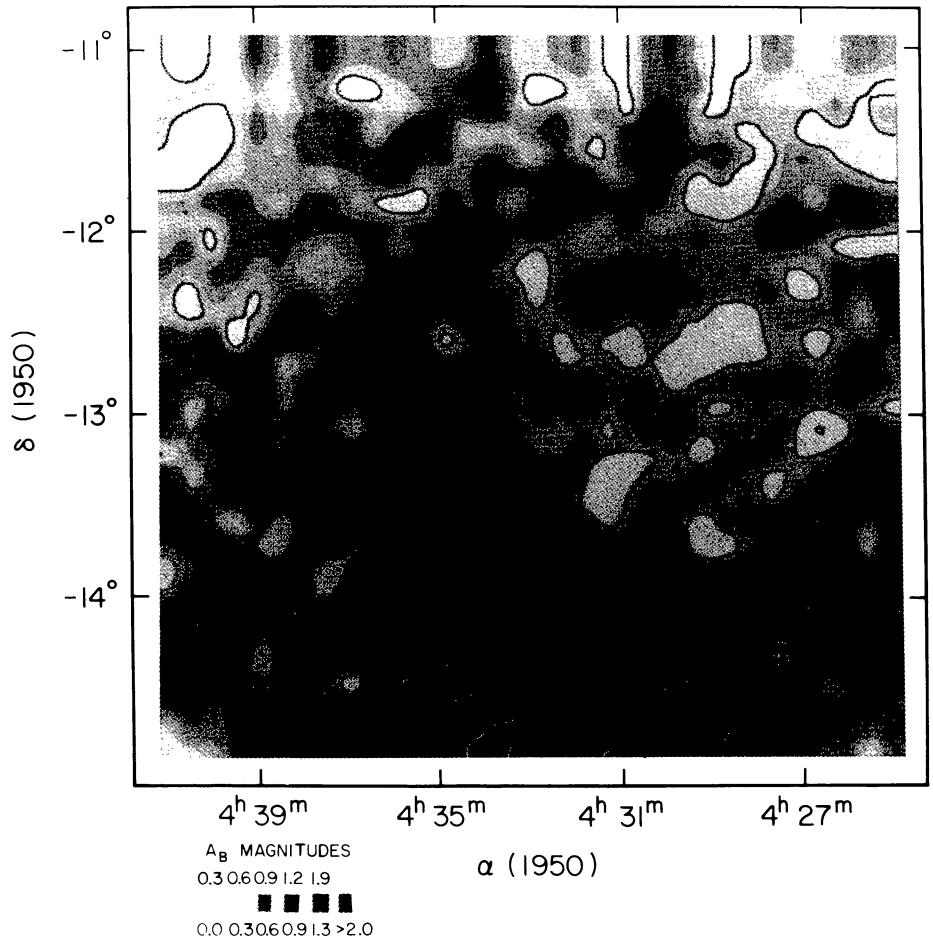

Fig. 3d. Same as Fig. 3a but for the region containing a portion of cloud 20 (also known as L 1642)

identifying foreground and background stars of known distances (e.g. Hobbs et al., 1986).

3. Results

The Wolf diagram technique was applied to seven of the high latitude molecular clouds. The objects chosen from the catalog in Paper II were those with the highest extinction in their central areas as determined from H_2 column densities obtained with the Bohlin et al. (1978) conversion factor. Table 2 lists the digitized regions, the cloud position based on CO or IRAS data, the distance from star counts, the extinction in visual magnitudes averaged over the region employed as the obscured area using both the magnitude 17 and brighter data and the full star count data, and the averaged visual extinction over the entire cloud as defined by the lowest contour ($0.5\,\mathrm{K\,km\,s^{-1}}$ integrated antenna temperature) of the CO(1 − 0) data from Paper II.

The goodness of fit parameter is examined along with the Wolf diagrams themselves to determine the distance as described above. There are two cases which arise with the use of the goodness of fit criterion: 1) The goodness of fit parameter shows a minimum at some value of the distance, or 2) the best fit to the data occurs at 50 pc and the goodness of fit parameter deteriorates with increasing distance. In the event that no minimum occurs, the first and second derivatives of the goodness of fit parameter are used to choose an upper limit to the distance of the obscuring cloud. The upper limit is chosen as that distance between the 50 pc intervals where the magnitude of the first derivative of the goodness of fit parameter increases by a factor of two or more. The upper limits chosen by this criterion also correspond to the distances at which the fit becomes noticeably poorer when examined by eye.

To eliminate the possibly deleterious effects of the upturns in the star count data at the fainter stellar magnitudes, two magnitude cutoffs (one at magnitude 15, hereinafter 15^m data, and one at magnitude 17, hereinafter 17^m data) are used to eliminate stars fainter than the cutoff magnitude from the data. The goodness of fit parameter for the various clouds is given in Table 3 for a best fit extinction (averaged over the obscured region) and for distances at 50 pc intervals for both magnitude cutoffs. We discuss the distance and extinction results individually for each scanned region:

Clouds 7 and 8: located near the Taurus region, these clouds may be fragments connected with the southernmost extension of that nearby molecular complex. The goodness of fit parameter for both the magnitude 15^m and 17^m data shows a minimum at a distance of 100–150 pc with the fit worsening considerably at lesser and greater distances as judged by eye estimates and factor of two changes in the first and second derivative of the parameter. Consequently, we adopt a distance of 125 pc for this cloud. The distance determined from the Wolf diagrams agrees with the distance to the Taurus dark clouds quoted by Elias (1978). Figure 4 shows the Wolf diagram for the obscured region for a distance of 100 pc and a blue extinction of $1\overset{m}{.}15$.

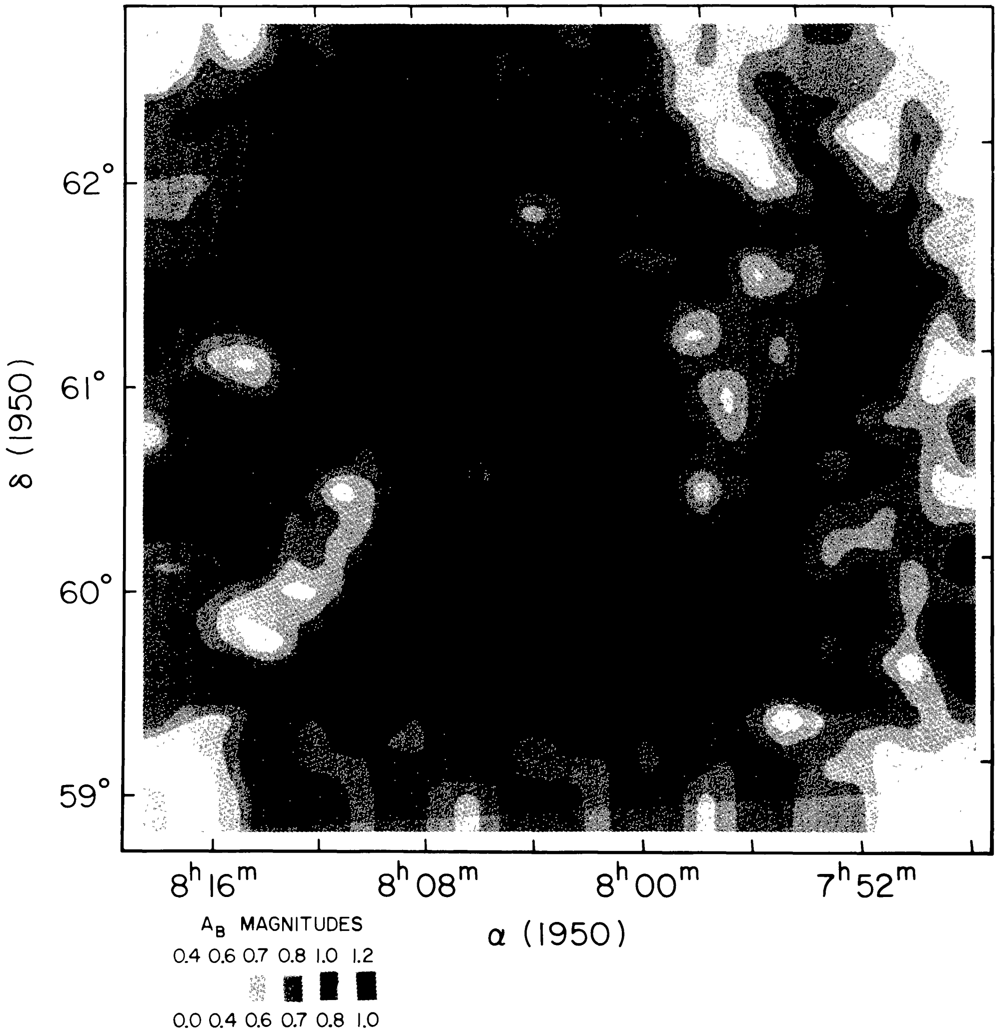

Fig. 3e. Same as Fig. 3a but for the region containing cloud 26

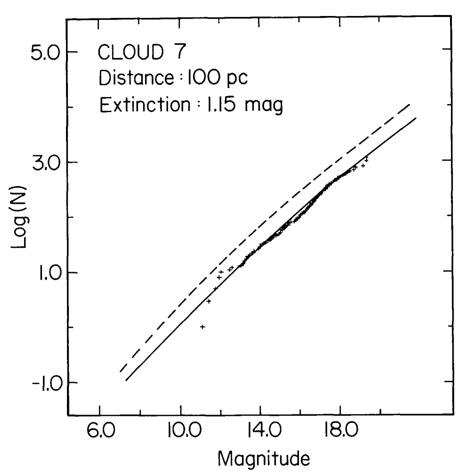

Fig. 4. Wolf diagram for a 0.5 square degree region in cloud 7. The dashed line is as described in Fig. 1. The crosses represent the actual star count data and the solid line represents a model obscuring cloud with a distance of 100 pc and $A_B \sim 1^m15$

The extinction to the 0.5 square degreee area chosen as the obscured field is $0^m9\,A_v$ using the 17^m data and $0^m7\,A_v$ using the full star count data. The area enclosed by the lowest CO contour shows an average extinction of $0^m5\,A_v$ and is shown in Fig. 3a.

Cloud 16: a large cloud ($3° \times 2°$) located near the Taurus region. As with clouds 7 and 8, IRAS data indicate that this complex may be associated with the Taurus molecular complex. An examination of the IRAS 100 μm data for this region shows low level (10 MJy ster^{-1}) emission extending south of the Taurus dark clouds to a latitude of $-45°$. Cloud 16 appears as an area of greater 100 μm emission (20–40 MJy ster^{-1}) embedded in the low level emission. Although the 15^m data show no minimum in the goodness of fit parameter for this object, the parameter significantly deteriorates for distances of 100 or more parsecs. The 17^m data show a minimum in the parameter at a distance of 100 pc with the fit deteriorating significantly at distances $\geqq 200$ pc. We adopt a distance of ~ 100 pc for this region. This estimate is also consistent with the distance to the Taurus region.

The Wolf diagrams for this cloud are based on an obscured region 1.0 square degrees in area and are the worst examples of the increase in the star counts at the faint magnitude end of the diagram (see Fig. 5). Using a smaller area (0.5 square degrees) of greater extinction did not remove the upturn in the data. However, using only the 15^m and 17^m star count data, the Wolf diagrams

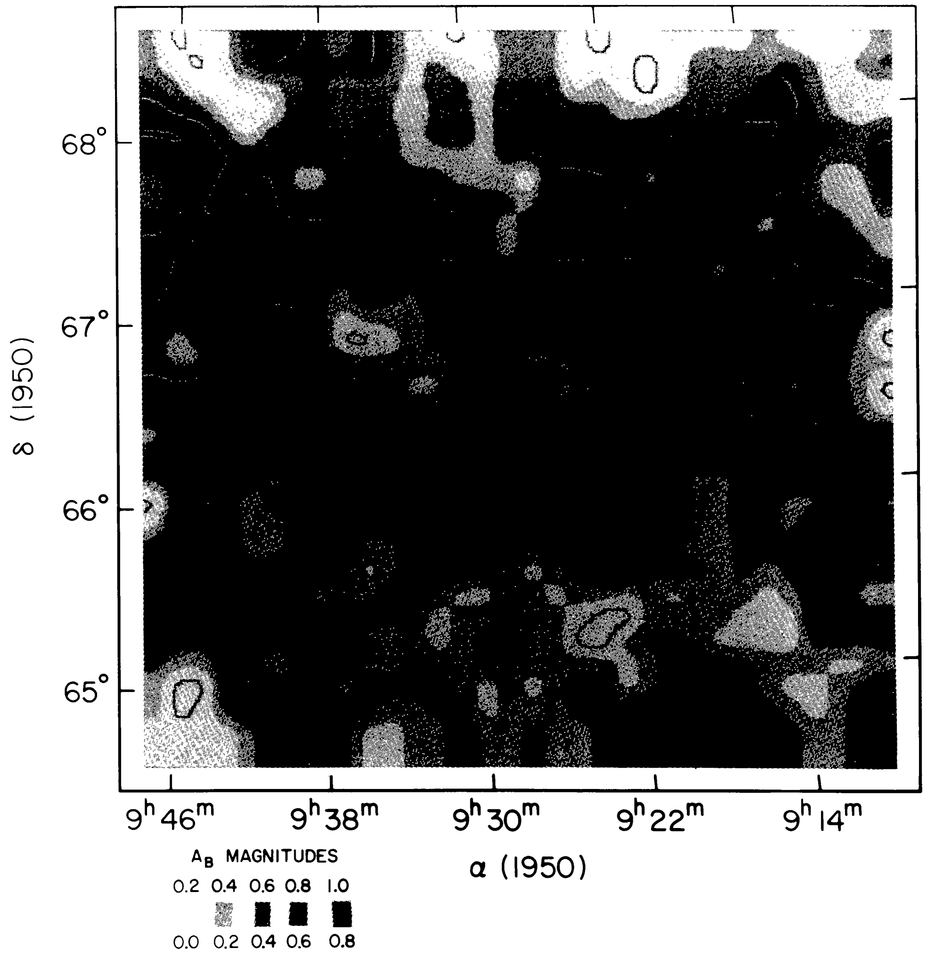

Fig. 3f. Same as Fig. 3a but for the region containing clouds 31 and 32

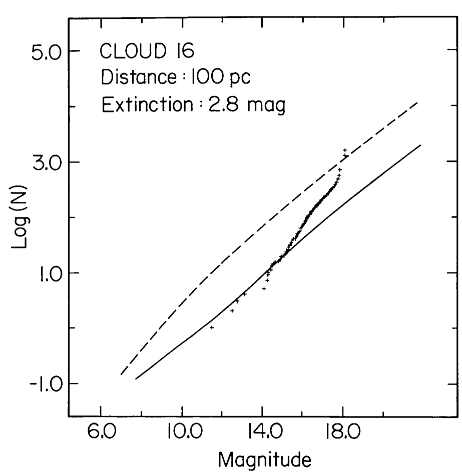

Fig. 5. Wolf diagram for a 0.5 square degree region in cloud 16. The symbols are as in Fig. 4 but with a model obscuring cloud at a distance of 100 pc and $A_B \sim 2\overset{m}{.}8$

even for cloud 16 are well-behaved and indicate that it is a local object.

This cloud shows the highest extinction among the digitized regions (see Fig. 3b). The discrepancy between the extinction obtained with the 17^m data and the total data is also greatest for this cloud; the 17^m data and the full star count data yield $A_v \sim 1\overset{m}{.}9$ and $1\overset{m}{.}4$ respectively. Despite the discrepancy between the two extinction measures, the extinction in the most obscured region of cloud 16 is low compared to the equivalent region in typical dust clouds ($1.5 < A_v \leqq 10$; Dickman, 1978a). The extinction averaged over the cloud within the lowest CO boundary is $0\overset{m}{.}7\ A_v$.

Cloud 18: also known as L 1569 (Lynds, 1962), this object is recognizable immediately on the POSS prints. However, star counts show less extinction in its central regions than the most obscured portions of cloud 16 which is not a Lynds (1962) dark nebula. The goodness of fit parameter based on a 0.75 square degrees area shows a minimum value at 50 pc and worsens significantly between 100 and 150 pc for the 15^m data and between 150 and 200 pc for the 17^m data. We adopt an upper limit to the distance of 175 pc for this complex. This object is also near the Taurus molecular complex, and as in the case of cloud 16, it is embedded in the low level 100 μm emission region. The distance estimate further supports the association of this object with the Taurus region.

The extinction in the area chosen as the obscured region is $1\overset{m}{.}1\ A_v$ with the 17^m data and $0\overset{m}{.}8\ A_v$ with the total star count data.

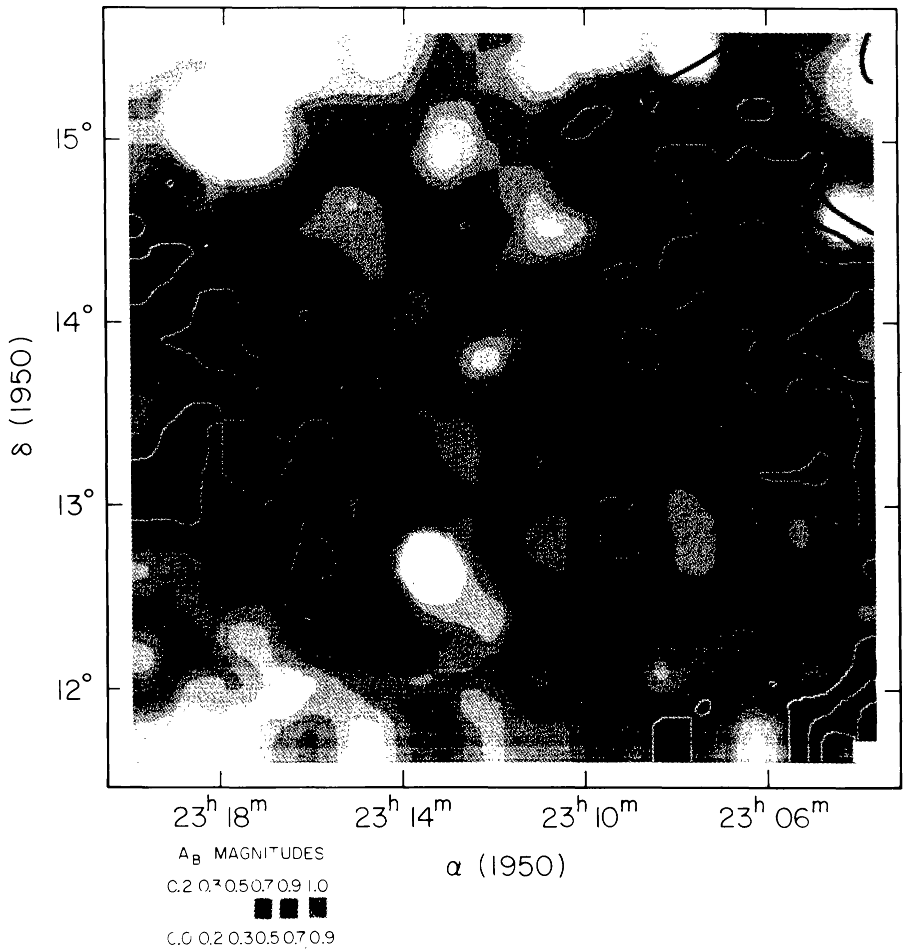

Fig. 3g. Same as Fig. 3a but for the region containing a portion of cloud 55. The lower right corner of the map ($\alpha < 23^h06^m$ and $\delta \sim 12°$) was not scanned and represents missing data

The entire molecular region shows an averaged extinction of $0\overset{m}{.}8\ A_v$ and is shown in Fig. 3c.

Cloud 20: also known as L 1642 (Lynds, 1962). The high extinction core of this cloud is clearly discernible on a POSS print and it exhibits a cometary nebula (Sandell et al., 1981) which has been identified with a pair of T Tauri stars (Sandell et al. 1986). The goodness of fit parameter shows a minimum of 50 pc for both sets of data. The fit deteriorates significantly between 50 and 100 pc for the 15^m data and between 100 and 150 pc for the 17^m data. This implies a distance of $\leqq 75$ pc based on the 15^m data and $\leqq 125$ pc for the 17^m data. We therefore adopt an upper limit to the distance of 125 pc for this cloud with the proviso that this object could be much closer than 125 pc. If the object is indeed closer than 125 pc, the presence of the T Tauri stars near the center of the nebula could make this the region of star formation nearest to the Sun.

The extinction to this object has also been presented in Sandell (1981) and compares favorably with our results. We obtain an extinction of $1\overset{m}{.}8\ A_v$ for the central 0.5 square degrees area chosen as the obscured region. The full extent of the molecular emission has not been fully determined, but within our mapped region the extinction is $0\overset{m}{.}8\ A_v$ (see Fig. 3d).

Cloud 26: one of seven high latitude clouds located in the IRAS 100 μm cirrus structure centered at $l = 143°$ and $b = 38°$ (the others are clouds 27–32; see Paper II). The goodness of fit parameter shows a minimum at 150 to 200 pc for both the 15^m and 17^m data. The first derivative of the best fit parameter begins to worsen substantially after a distance of 200 pc. Although it is difficult to tell how distant this object is, the Wolf diagrams and the best fit parameter indicate that the object is 150 to 200 pc from the Sun; we therefore adopt a distance of ~ 175 pc for this cloud.

The extinction in the central region of this cloud is $0\overset{m}{.}6\ A_v$ as determined from both the 17^m data and the total star count data. Within the CO cloud boundary (see Fig. 3e) the extinction is $0\overset{m}{.}7\ A_v$. This result is due to the discrete nature of the area chosen as the obscured region; because of computing considerations, the obscured region is composed of rectangular grids. Although we attempted to choose only those grids which are located on the most obscured portion of the cloud, in some instances one of the rectangular grids also contains a less obscured region, thereby lowering the average extinction in the obscured field of the Wolf diagram.

Clouds 31 and 32: part of the cirrus region mentioned above. Like cloud 26, these clouds are low extinction objects. Even an area of only 0.5 square degrees yields an average extinction of $0\overset{m}{.}5\ A_v$. As in the case of cloud 26 above, the low extinction and the paucity of stars brighter than thirteenth magnitude render a distance determination difficult. The goodness of fit parameter does not show a minimum and does not deteriorate significantly until distances of 150–200 pc for the 15^m data and 250–300 pc for the 17^m data. We adopt an upper limit to the distance of $\leqq 275$ pc, consistent with the distance to the related cloud 26.

As with cloud 26, the extinction to this object is very low, $0\overset{m}{.}4\ A_v$ for the 0.5 square degrees area chosen as the obscured field and $0\overset{m}{.}3\ A_v$ for the area enclosed by the lowest CO contour (see

Fig. 3f). The extinction averaged over the region of molecular emission is the lowest of any of the clouds studied and is close to the value of extinction necessary to produce a transition in the total H column density from small ($<10^{16}\,\mathrm{cm}^{-2}$) to large ($>10^{19}\,\mathrm{cm}^{-2}$) values of H_2 (Savage et al., 1977).

Cloud 55: part of a large loop structure revealed by IRAS 100 μm data and centered at $l = 93°$ and $b = -38°$. This structure is also clearly visible on the H I maps of Heiles (1984; plate 23). The low extinction in the 0.75 square degrees area chosen as the obscured field ($A_v \sim 0\overset{m}{.}5$) coupled with a slight rise in the m versus $\log N(m)$ curve at magnitude 14 make the star count results very difficult to interpret. The goodness of fit parameter worsens substantially at distances greater than 150 pc for both the 15^m and for the 17^m data. We adopt an upper limit of 175 pc for the distance of this cloud. The Wolf diagram for this region is shown in Fig. 10 for a cloud with $A_B \sim 0\overset{m}{.}7$ and a distance of 150 pc.

The extinction averaged over the molecular portion of the cloud within the scanned region is only $0\overset{m}{.}4\, A_v$ (see Fig. 3g). Although this object is the largest high latitude molecular cloud in spatial extent (>5 square degrees as determined from the CO (1 − 0) emission), the extinction is very low and thus the entire cloud is particularly difficult to identify visually on the POSS prints. The core region shows an integrated (CO (1 − 0) line profile greater than $17\,\mathrm{K\,km\,s^{-1}}$ and a visual extinction of only $0\overset{m}{.}8$. This effect is due in part to the differences in resolution of the CO and the extinction data (2ʹ.3 and 8ʹ respectively) and is perhaps an indication that the extinction is very patchy on small angular scales.

An accurate distance determination to this complex is important because of its large spatial extent. To check the validity of the above distance estimate, star counts were conducted in a nearby region centered at $\alpha = 23^h50\overset{m}{.}7$ and $\delta = 20°40'$ and termed cloud 55A. The IRAS data show 100 μm emission in this region comparable to the emission along the main body of cloud 55.

Cloud 55A: as for cloud 55, the 0.5 square degrees area chosen is a low extinction region ($A_v \sim 0\overset{m}{.}5$) so that the turnoff in the Wolf diagrams is not evident. For both the 15^m and the 17^m data, there is no minimum in the goodness of fit parameter. There appears to be a significant change in the parameter at distances greater than 150 pc for the 15^m data and at distances greater than 250 pc for the 17^m data. We adopt an upper limit to the distance of this cloud of ≦275 pc with perhaps an upper limit of ≦175 pc possible.

Because this object is not mapped in CO, we cannot estimate the extinction averaged over the molecular portions of the cloud. However, the star counts do not show any regions of high extinction in the scanned area, implying that any molecular material in this region will exhibit extinction similar to the other high latitude molecular clouds.

4. Conclusions

Star counts from POSS plates confirm that the high latitude molecular clouds are indeed nearby objects. Distances to three of the objects are determined and range from ~100 pc to ~175 pc; for five other objects we determine upper limits to the distance ranging from ≦125 pc to ≦275 pc. Our results are consistent with the determinations in Papers I and II based on the velocity dispersion of the ensemble of clouds that the average distance to the clouds is about 100 pc. These two independent distance estimates firmly locate the high latitude molecular clouds in the local interstellar medium. These objects as a group are the nearest molecular clouds to the Sun and as such, they are excellent candidates for high resolution studies.

Because the high latitude molecular clouds are always associated with the cores of IRAS infrared cirrus (Weiland et al., 1986) the distance estimates in this paper locate at least some of the cirrus in the local solar neighbourhood.

Cloud 20, which harbors a pair of T-Tauri stars, is located at a distance of <125 pc and may be nearer than 75 pc. Distance estimates based on interstellar absorption lines may better determine the distance to this object. If it is closer than 125 pc it is the nearest known star forming region.

The extinctions averaged over the area enclosed by the lowest CO(1 − 0) contour from the data in Paper II are very low: A_v ranges from $0\overset{m}{.}3$ to $0\overset{m}{.}9$. These values are within a factor of two of the values calculated in Paper II from the integrated intensity averaged over the face of a cloud. The 0.4 to 1 square degrees areas chosen as the obscured regions show greater extinction; A_v ranges from $0\overset{m}{.}45$ to $2\overset{m}{.}1$. However, these values are still much smaller than values obtained in the core regions of typical dark clouds which range from $1\overset{m}{.}5$ to $10^m\, A_v$ (Dickman, 1978 a). The objects chosen for this study are the high latitude clouds exhibiting the greatest H_2 column density in their central regions. The other high latitude clouds most likely will have lower extinction averaged over the area of molecular emission. A typical high latitude molecular cloud thus appears to have an average visual extinction of $\leqq 0\overset{m}{.}5$.

Acknowledgements. We would like to thank the Sterrewacht Leiden for providing the hospitality, computer time, and facilities necessary to carry out this project. We thank Dr. Leo Blitz and an anonymous referee for a critical reading of the manuscript. One of us (L.M.) gratefully acknowledges support from NSF grant AST 83-15276.

References

Adolfsson, T.: 1955, *Arkiv for Astronomi* **1**, 495

van Albada, G.D., Baud, B., de Pagter, P.J., Pol, W., Renes, J.J.: 1985, ROG Internal Report

Allen, C.W.: 1973, *Astrophysical Quantities*, 3rd eds. The Athlone Press, London

Bahcall, J.N., Soneira, R.M.: 1980, *Astrophys. J. Suppl. Series* **44**, 73

Blitz, L., Magnani, L., Mundy, L.: 1984, *Astrophys. J. Letters* **282**, L9 (Paper I)

Bloemen, J.B.G.M., Caraveo, P.A., Hermsen, W., Lebrun, F., Maddalena, R.J., Strong, A.W., Thaddeus, P.: 1984, *Astron. Astrophys.* **139**, 37

Bohlin, R.C., Savage, B.D., Drake, J.F.: 1978, *Astrophys. J.* **224**, 132

Bok, B.: 1937, *The Distribution of Stars in Space*, University of Chicago Press, Chicago

Brandt, J.C., Stecher, T.P., Crawford, D.L., Maran, S.P.: 1971, *Astrophys. J. Letters* **163**, L99

Dickman, R.L.: 1978a, *Astrophys. J. Suppl.* **37**, 407

Dickman, R.L.: 1978b, *Astron. J.* **83**, 363

Elias, J.H.: 1978, *Astrophys. J.* **224**, 857

Heiles, C.: 1984, *Astrophys. J. Suppl.* **55**, 585

Hobbs, L.M., Blitz, L., Magnani, L.: 1986, *Astrophys. J. Letters* **306**, L109

Jarvis, J.F., Tyson, J.A.: 1981, *Astron. J.* **86**, 476

Lebrun, F.: 1986, *Astrophys. J.* **306**, 16
Low, F.J., Beintema, D.A., Gautier, T.N., Gillett, F.C., Beichman, C.A., Neugebauer, G., Young, E., Aumann, H.H., Boggess, N., Emerson, J.P., Habing, H.J., Hauser, M.G., Houck, J.R., Rowan-Robinson, M., Soifer, B.T., Walker, R.G., Wesselius, P.R.: 1984, *Astrophys. J. Letters* **278**, L19
Lynds, B.T.: 1962, *Astrophys. J. Suppl.* **7**, 1
McCuskey, S.W.: 1941, *Astrophys. J.* **94**, 468
Magnani, L., Blitz, L., Mundy, L.: 1985, *Astrophys. J.* **292**, 402 (Paper II)
Magnani, L., Blitz, L., Wouterloot, J.G.A.: 1986 (in preparation)
van Rhijn, P.J.: 1929, *Groningen Pub.*, Vol. 43
Sandell, G., Johannson, L.E.B., Nguyen-Q-Rieu, Mattila, K.: 1981, *Astron. Astrophys.* **97**, 317
Sandell, G., Reipurth, B., Gahm, G.: 1986 (in preparation)
Savage, B.D., Bohlin, R.C., Drake, J.J., Budich, W.: 1977, *Astrophys. J.* **216**, 291
Swaans, L.: 1981, Ph. D. Thesis, Sterrewacht Leiden
de Vries, C.P.: 1984, *Astronomical Photography 1984*, eds. E. Sim, K. Ishida, in Reports ROE, No. 14, p. 311
de Vries, C.P.: 1986, Ph. D. Thesis, Sterrewacht Leiden
Weiland, J., Blitz, L., Dwek, E., Hauser, M.G., Magnani, L., Rickard, L.J.: 1986, *Astrophys. J. Letters* **306**, L101
Wolf, M.: 1923, *Astron. Nachr.* **219**, 109